Modelling of Electro-Rheological Dampers for Automotive Suspensions: Healthy and Faulty Cases

Marcelo Menezes Morato, Thanh-Phong Pham, Manuel Alejandro Molina Villa, Olivier Sename, Luc Dugard

Modelling of Electro-Rheological Dampers for Automotive Suspensions: Healthy and Faulty Cases

Marcelo Menezes Morato[a,b], Thanh-Phong Pham[b,c], Manuel Alejandro Molina Villa[b], Olivier Sename[b], Luc Dugard[b]

[a] *Departamento de Automação e Sistemas (*DAS*), Universidade Federal de Santa Catarina, Florianópolis, Brazil.*
[b] *Univ. Grenoble Alpes, CNRS, Grenoble INP$^{\top}$, GIPSA-lab, 38000 Grenoble, France.*
$^{\top}$ *Institute of Engineering Univ. Grenoble Alpes*
[c] *Faculty of Electrical and Electronic Engineering, University of Technology and Education, The University of Danang, 550000 Danang, Vietnam*

Abstract

This work presents a thorough modelling study of Electro-Rheological (*ER*) Dampers used in vehicle suspension systems. The main purpose is to consider the overall behaviour of these *ER* dampers, which basically, present a resistance against shearing that varies according to a controlled electric field. This study is a two-fold: *i)* the first part is an analytical approach towards the dynamical modelling of the *ER* damper force, wherein a conclusive parametric model is obtained; *ii)* the second part aims to analyze and model the possibility of faults upon the dampers which is of paramount importance for suspension system diagnosis and reliability. Throughout this study, simulation and experimental validation results from a real mechatronic test bench are presented. The overall results assess the ability and the accuracy of the proposed model to characterize the force delivered by *ER* dampers in both healthy and faulty situations.

Keywords: Electro-Rheological Dampers, Modelling, Identification, Fault Analysis, Experimental Faults.

Email addresses: marcelomnzm@gmail.com (Marcelo Menezes Morato), thanh-phong.pham2@gipsa-lab.grenoble-inp.fr (Thanh-Phong Pham), mmolina2127@gmail.com (Manuel Alejandro Molina Villa), olivier.sename@gipsa-lab.fr (Olivier Sename), luc.dugard@gipsa-lab.fr (Luc Dugard)

1. Introduction

Through recent years, the automobile market has always been waiting for product new developments in order to improve driving performances and passengers comfort. It is important to highlight that there exists a great variety of vehicles with specific goals, behaviours and performances. Nonetheless, the mechanical structures of automotive systems are mostly the same, as detailed in [12]. To handle new market requirements, technological improvements of each component of a vehicle are of high interest for the whole car industry. This paper is focused on the study of new suspension technologies.

1.1. Automotive Suspension Systems

A vehicle's suspension system usually consists of three main elements: an elastic structure, a shock absorber (the damping system) and a set of mechanical parts. Typically, the elasticity comes from a coil spring that delivers a force proportional and opposite to the suspension deflection - this structure carries all the static load but it increases the vehicle's oscillations. The damping element is, then, added to reduce this oscillation effect by delivering a dissipative force proportional and opposite to the deflection speed. Finally, the set of mechanical elements links the body (chassis of the vehicle) to the unsprung mass (wheel), as described in [39], as illustrated in Figure 1.

Essentially, a vehicle's suspension system supports the weight of the upper part of the vehicle on its axles and wheels, allows the vehicle to move over irregular surfaces with a minimum of body trepidation (stability), reduces the load transferred from road (ride comfort) and enables the vehicle to corner with minimum roll or loss of traction between the tires and the road (good handling). Good ride comfort requires a soft suspension, whereas the stability of the vehicle requires a hard suspension. In terms of good handling, a suspension with an intermediate setting in between the two is required. Normally, if the system has gains in terms of comfort, it looses in terms of handling performance, as they are known to be contradictory objectives, as stated in [19].

Improvements have been recently brought for these systems. For exemple, an *Active* suspension is a type of suspension that is able to precisely control the vertical movement of the wheels relative to the chassis, which is not the case for a passive suspension [45]. Active suspensions are generally divided into two main classes: purely active and semi-active ones, see [38]. In [43] it is shown that, while the latter ones only vary the shock absorber characteristics

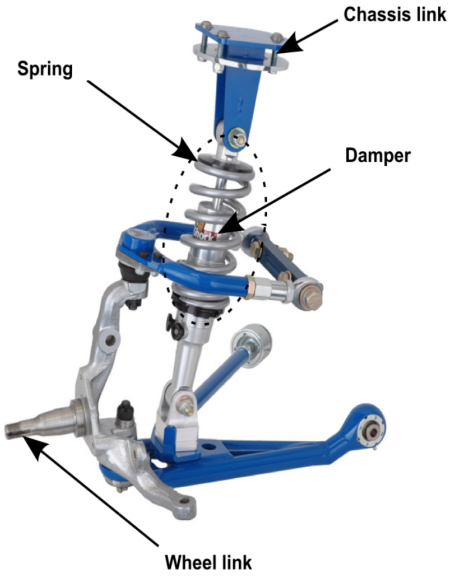

Figure 1: Schematic Representation of a Common Vehicle Suspension System [39]

to match changing road or dynamic conditions, the first ones act to raise and lower the chassis independently at each wheel.

Being able to overcome the limitations of a passive suspension system, active suspensions have been developed and applied in various practical applications and in industrial *top*-cars (*Formula* 1, *etc*), see [13] and [36]. With an additional active force introduced as a part of a suspension unit, the system is controlled using appropriate algorithms to make it more responsive to various road profiles. However, this type of suspension requires high power sources, active actuators, sensors and sophisticated control logics. Otherwise, a semi-active configuration can address these limitations by effectively integrating a tuning control scheme with adjustable passive devices, wherein active force generators are replaced by modulated variable compartments, such as a variable rate damper, see [39]. Semi-active suspension can feature an electronic shock absorber that may vary the damping with a relatively large bandwidth. The forces are delivered according to the passivity constraint of each damper, which means that no energy is introduced into the system, but only dissipated. Due to these features, the energy to power these suspensions is very low, compared to the one dissipated by purely active dampers.

1.2. Electro-Rheological Dampers

Commonly, semi-active suspensions with controlled fluids are the most used ones, since they have fast time response and are less costly. These systems can achieve the optimal compromise between ride comfort and road handling for several road scenarios, as analyzed in [10] and references therein. Such a fast variation of damping may be achieved by the three following technologies: Electro-Hydraulic (EH) dampers, hydraulic devices usually equipped with solenoid valves [2]; Magneto-Rheological (MR) and Electro-Rheological (ER) schock absorbers, dampers filled with Rheological fluid that varies its viscosity under the action of a magnetic or an electric field, respectively.

In terms of EH and MR dampers, the following references should be mentioned: the modelling and experimental identification of MR dampers have been recently seen in [31], [12] and [1]; EH semi-active dampers have been studied in [46].

The use of ER dampers in semi-active suspension systems is analysed in [8], wherein results show that both ride comfort and steering ability (roll and pitch motion reduction) of the vehicle can be significantly improved with these elements. With the aid of high-fidelity simulations, [24] shows a study of ER dampers with digitally controlled valves and their application to automotive systems.

Then, the purpose of this work is to analyze and model the behaviour of the force delivered by Electro-Rheological dampers, shock absorbers wherein a duty fluid presents a resistance against shearing that varies together with the electric field applied over it. To do so, this work will consider both healthy and faulty states of the damper which, as far as the authors know, is new in literature.

1.3. Related Works

In terms of damper's modelling, recent works have presented two main approaches: parametric and non-parametric modelling.

In terms of non-parametric modelling, a damper is characterized by special, well-suited functions (polynomial, trigonometric, delayed functions, *etc*) or artificial intelligence methods (fuzzy logics, neural networks, *etc*). From literature, the following contributions can be cited:

- A phenomenological technique to model automotive dampers is detailed in [40];

- Then, in [25], a large scaled *MR* damper is modelled according to this same technique;
- A polynomial function is used to described the behaviour of the force delivered by a damper due to its piston's velocity in [11];
- To describe the friction damping behaviour of joints, a non-parametric trigonometric model is proposed in [17];
- In [15], an Electro-Rheological fluid's behaviour is modelled with the use of *Chebychev* polynomials;
- A similar method to model a complete *ER* device is given in [30].

The difficulties of non-parametric models is that, often, the resulting function that describes a damper's behaviour is quite complex.

This work will focus on *ER* damper modelling using a parametric approach. In this type of approach, a damper is characterized by the combination of linear and nonlinear elements that define individually the behaviours of the spring, dashpots and other mechanical parts, detailing their mechanisms and operating area, as first seen in [14]. Some other works using the parametric approach for modelling can be mentioned:

- To describe the behaviour of controllable fluids and, specifically, damper fluids, a parametric model is developed in [16];
- Using basic mechanical laws, [23] and also [27] have developed parametric models to characterize *ER* fluids and devices;
- A non-linear parametric model, based on simple mechanical idealizations, has been discussed by a group of authors in [41] and [42];
- Parametric dynamical modelling of *ER* materials with a frequency analysis is presented in [16].

However, while a faulty behavior of semi-active dampers could be very detrimental to the vehicle performances, this problem has been very little considered. Some first results are presented in [20] concerning the oil leakage issue.

1.4. Main Objectives and Contributions

Given the unavailability of a conclusive and well-validated model of *ER* dampers in faulty and healthy situations, the article's main goals are:

- To describe and elaborate a complete dynamical model of an Electro-Rheological damper, which is essential to well implement new control strategies for semi-active suspension systems. This is a rather open topic in literature, up to the authors knowledge, since most models of *ER* dampers are mainly adapted from models of *MR* dampers or are purely static models.
- To identify the model parameters using linear and nonlinear identification methods.
- To validate the achieved model with experimental tests, proving its accuracy.
- Furthermore, this work aims to analyze and model several fault scenarios that might occur for the Electro-Rheological dampers, a new topic in literature, up to the authors knowledge. This allows the development of a platform that tests different kinds of faults affecting real *ER* dampers. Moreover, this study is completed by experimental results with a dedicated ER damper mounted on a scaled vehicle 4-poster bench.

1.5. Organisation of the Paper

The paper is organized as follows: firstly, in Section 2, some preliminaries and the vehicle test-rig are presented; then, in Section 3, the analysis of *ER* dampers is detailed, which leads to a parametrical model of the complete behaviour of these shock absorbers. This is followed by the model identification procedure, given in Section 4; Section 5 presents the results in terms of fault modelling for *ER* dampers. Then, in Section 6, different ways to simulate the studied faults on real experimental testbeds are described. Finally, conclusions are drawn in Section 7.

2. Experimental INOVE platform

For validation and identification goals, as well as for many experimental tests, a real $\frac{1}{5}$-sized vehicle test rig is used in this work. This testbed is the

INOVE Soben-Car experimental platform (see Figure 2) that allows dealing with several configurations and use cases - for full details refer to [45] and [44]. It is available in GIPSA-lab (http://www.gipsa-lab.fr/projet/inove/index.html)

Figure 2: *INOVE Soben-Car* Test-Bench

This car is equipped with a Semi-Active suspension system involving four *ER* dampers which have a force range of $\pm\,50\,\mathrm{N}$. These dampers are adjusted using a controlled voltage inside the range of $[0\,,\,5]\,\mathrm{kV}$, generated by amplifier modules. The control input for each module is a *PWM* signal at $25\,\mathrm{kHz}$. In terms of capturing the vehicle's behaviour, this testbed is equipped with a wide variety of sensors, like relative displacement sensors to measure the deflection of each *ER* damper and force sensors to measure the dampers' forces. A photo of the front-left *ER* damper of the experimental platform is given in Figure 3.

Figure 3: Electro-Rheological Damper on *INOVE Soben-Car* Test-Bench

In order to characterize these dampers, a first steady-state analysis is done, considering a fixed electric field setting and sinusoidal bumps for the road profile. The damping force increases until reaching a constant level and the stationary value of damping force is recorded. The same procedure is done for different velocity profiles within the interval of $[-0.15\,,\,0.15]\,\frac{\mathrm{m}}{\mathrm{s}}$, considering that the applied tension $(U(t))$ is taken as fixed values in the interval of $[0\,,\,1.5]\,\mathrm{kV}$. In Figure (4), real data of *ER* damper are drawn, with a Force vs. Deflection plot and a Force vs. Deflection Velocity diagram.

3. Modelling of an *ER* Damper

This section explores the details of the behaviour of Electro-Rheological shock absorbers. The main objective is to propose an analytical approach to model the *ER* damper force that will be used especially in control-oriented models of vehicle suspensions.

First some background is given about Electro-Rheological dampers. As depicted in [7], where the control characteristics of *ER* dampers are analysed,

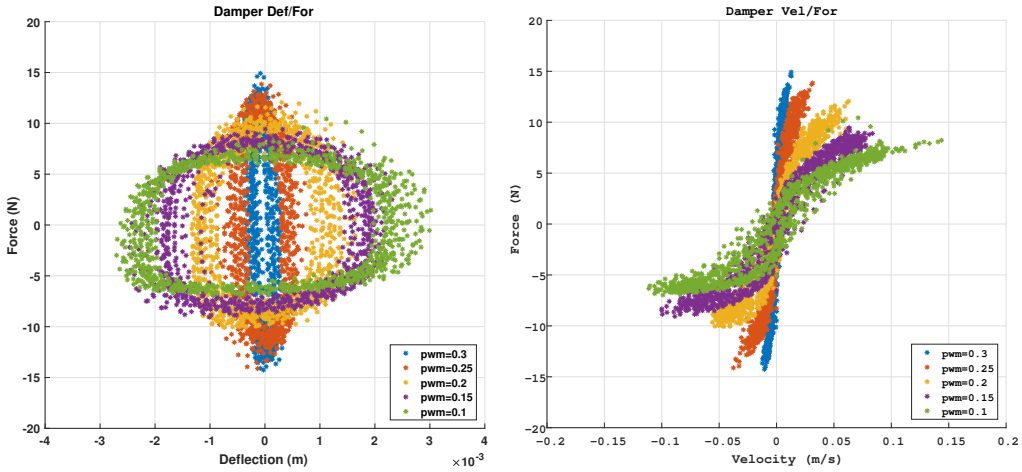

Figure 4: Experimental data of *ER* damper

these are often characterized by the use of two diagrams: the Force *vs.* Piston Displacement (suspension deflection) plot and also, the Force *vs.* Piston Velocity (suspension deflection velocity) plot. The expected forms of these two diagrams are given in Figure 5, as shown in [39].

Starting from the schematic configuration and operating principle of *ER* dampers, a *quasi*-static model is derived on the basis of the Bingham Rheological laws of *ER* fluid [5]. From this *quasi*-static model, a complete dynamic model for the *ER* damper is proposed. The dynamical model is derived from empirical behavior observations in various experiments on a real mechatronic testbed. To validate the obtained model, simulations are performed and the results are compared to real measured data (using force sensors).

3.1. Parametrical Static Model of ER *Dampers*

Firstly, the used model for the static behaviour of Electro-Rheological dampers, represented by the schematic diagram in Figure 6, is developed.

The fluid used in the *ER* shock absorbers is a colloidal suspension whose viscosity varies according to an applied external electric field. A complete study of these *ER* fluids is given in [22], in terms of sedimentation over usage, compliance due to impulse force response, shear stress behaviour and other characteristics. A discussion about the use of these fluids on damper devices is presented in [47], where vibration tests allow to illustrate the mechanism

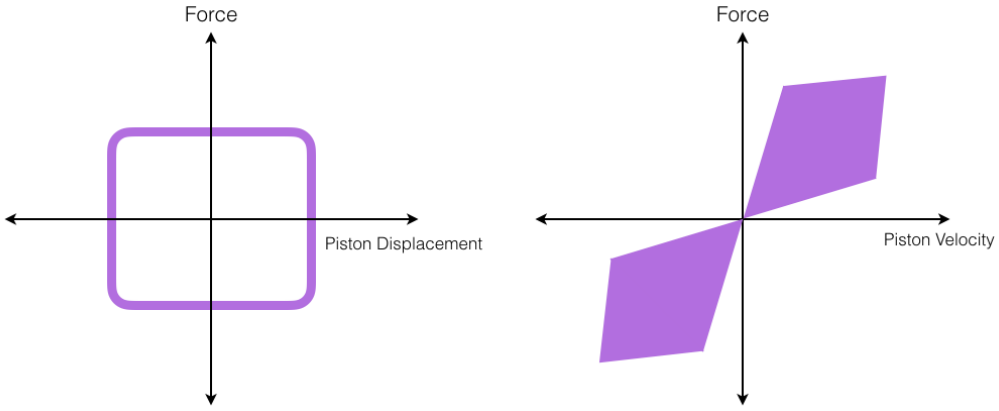

Figure 5: Expected Damper Characteristics

of the *ER* effect towards shock absorbing (acceleration transmissibility, influence of load on damping ration, stiffness and damping ability, *etc*). In [32] the analysis of the dynamics of *ER* fluid in *ER* clutches has been done. The analysis of the *ER* fluid's flow behaviour in steady-flow conditions has been done in [35], where a test rig is used to predict the flow's behaviour for constant values of electric field excitation. The results therein show that good predictions can be made in terms of the steady pressure loss versus the flowrate relationship at constant excitation.

The structure of *ER* dampers is divided into upper and lower chambers by a piston. These chambers are fully filled with the Rheological fluid. As the piston moves, the *ER* fluid flows from one chamber to the other through the annular duct between inner and outer cylinders. The inner cylinder is connected to a positive voltage produced by a high voltage supply unit, represented by the positive electrode (+). The outer cylinder is connected to the ground, represented as the negative electrode (−).

On the other hand, a gas chamber located outside the lower chamber acts as an accumulator of the *ER* fluid induced by the motion of the piston. In the absence of electric field, the *ER* shock absorber produces a damping force caused only by the viscous fluid resistance. However, if some electric field is applied to the *ER* damper, it produces an additional damping force owing to the yield stress of the *ER* fluid. This damping force can be continuously tuned by controlling the intensity of the applied electric field.

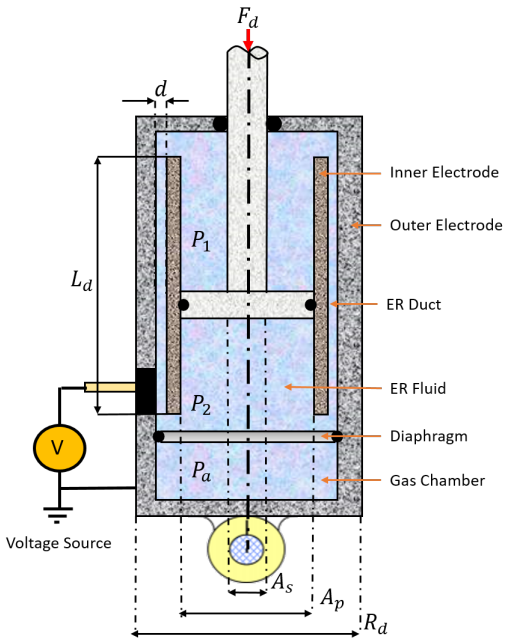

Figure 6: Schematic Representation of an *ER* Damper, adapted from [9]

The force generated by *ER* dampers, namely $F_d(t)$, depends on the difference of pressures between the chambers, that is related to the mechanical contact in each side of the piston. This relationship can be expressed in terms of the piston area (A_p) and the piston shaft area (A_s) as expressed below:

$$F_d(t) = P_2(t) \times A_p - P_1(t) \times (A_p - A_s) \tag{1}$$

The pressure inside the two chambers of the damper can be expressed in terms of the gas chamber pression (P_a). The pressure in the lower chamber (P_2) is equal to the gas chamber pression with a pressure drop ΔP_a between the chambers. Normally, these pressure drops are small and can be neglected. On the other hand, the pressure in the higher chamber (given by P_1) can be expressed as the gas chamber pressure with a pressure drop ΔP_d due to the *ER* fluid that flows through the annular duct, between the chambers. Thus, these pressures P_1 and P_2 can be expressed analytically as follows:

$$\begin{aligned} P_1(t) &= P_a(t) - \Delta P_d(t) \\ P_2(t) &= P_a(t) + \underbrace{\Delta P_a(t)}_{\approx 0} \approx P_a(t) \end{aligned} \tag{2}$$

Assumption 1. *The initial pressure in the system (*ER *damper) can be given in terms of the initial pressure of the gas chamber (P_0), a thermal expansion coefficient (γ), the initial gas volume (V_0) and its variation generated by the piston displacement ($x_p(t)$).*

This leads to the following expression:

$$P_a(t) \;=\; P_0 \times \left(\frac{V_0}{V_0 - A_s x_p(t)}\right)^{\gamma} \tag{3}$$

By replacing the expressions for the pressures from Equation (2) into Equation (1), it is possible to obtain a first analytical force model that takes into account the physical parameters of the damper. This expression is given in terms of the system's internal pressure, the contact areas of the piston and the pressure drop due to *ER* fluid that flows through the annular duct.

$$F_d(t) \;=\; P_a(t) \times A_s + \Delta P_d \times (A_p - A_s) \tag{4}$$

Now, the problem is to describe how this force models varies according to the changes upon the controllable electric field. The behavior of the *ER* fluid is quite peculiar, thanks to the possibility of change of its viscosity factor due to an electric field. This behavior is described by several models, but the *Bingham Model* (see [4]) is the most commonly used, as it is the most representative one. This model contemplates the description of two behaviours: a nominal behaviour of the fluid (without any external electric flied) and a controlled behaviour (with an external electric field). The total shear resistance of the fluid can be expressed as the addition of these two situations.

The nominal behavior can be given as the regular fluid friction between pipes. It depends on the flow rate (Q_d), the nominal viscosity of the fluid (μ) and the geometry of the pipe (length L_d, radius R_d and gap d) as follows:

$$\Delta P_d^{\text{nominal}}(t) \;=\; \frac{6\mu L_d}{\pi d^3 R_d} Q_d(t) \tag{5}$$

Concerning the behaviour of the fluid in the presence of an external electrical field, the (Bingham) model expresses the annular duct's pressure drop

in terms of the geometrical form of the duct, the flow velocity and the yield stress of the Rheological fluid induced by the applied electric field.

As stated in [7], the Rheological properties of *ER* fluids are reversibly changed with the application of an external electric field $E(t)$. From Newtonian flow behaviour, the *ER* fluid particles change to a Bingham plastic behaviour, in which particles become aligned in chain forms, according to the applied $E(t)$. In [7], a microphotography analysis of arabic gum-based *ER* fluid is given, comparing the *ER* fluid flow behaviour with and without the influence of an external electric field. The particles move freely when there is no electric field and in chains when there is. The Bingham plastic behaviour of the *ER* fluid flow is characterized by the fluid's shear stress (τ), in terms of the shear rate (flow rate), viscosity and yield stress due to the applied electric field. This is represented by the following Equation, as detailed in [21]:

$$\tau(t) \quad = \quad \mu Q_d(t) + \tau_y(t) \tag{6}$$

The fluid's shear stress $\tau(t)$ influence upon the pressure drop $\Delta P_d(t)$ derives from Equations (5) and (6). The yield stress (τ_y) is thus given by the expression seen in Equation (7), where $E(t)$ stands for the applied electric field and α and β represent intrinsic parameters of the *ER* fluid. Finally, the pressure drop ΔP_d can be given as in Equation (8), where c is a coefficient that stands for the fluid's flow velocity profile.

$$\tau_y(t) \quad = \quad \alpha E^{\beta}(t) \tag{7}$$

$$\Delta P_d(t) \quad = \quad \frac{6\mu L_d}{\pi d^3 R_d} Q_d(t) + \underbrace{c\frac{L_d}{d}\tau_y(t)}_{\text{Due to Electric Field}} \tag{8}$$

Remark 1. Herein, the piston's velocity $\dot{x}_p(t)$ is equivalent to the fluid's flow rate $Q_d(t)$.

Then, a final parametric static model is obtained. This model is given by Equation (9), where the first term represents the elastic force from the gas compliance, the second term represents the damping force due to *ER* fluid viscosity when no electric field is applied and the third one stands for the force due to the yield stress of the Rheological fluid, which can be continuously

controlled by the intensity of the electric field applied to the damper.

$$
\begin{aligned}
F_d(t) &= \overbrace{[P_a(t)A_s]}^{\text{Gas compliance}} + \overbrace{\left[\frac{6\mu L_d}{\pi d^3 R_d}\dot{x}_p(t)\right]}^{ER\text{ Viscosity}} \\
&+ \overbrace{\underbrace{(A_p - A_s)\frac{cL_d}{d}\alpha E^{\beta}(t)\,\text{sign}\{\dot{x}_p(t)\}}_{\text{Yield stress}}}^{F_{ER}(t)}
\end{aligned} \tag{9}
$$

Remark 2. The term "sign$\{\dot{x}_p(t)\}$" appears in the Yield Stress term of the damper force $F_d(t)$, given that the force's direction depends on the direction of the piston's velocity, if there is a compression or a release movement (thus if it is postive or negative).

This model has been statically validated as proposed in [37]. Therefore, the validation of model (9) is done by considering as the input the piston rod's velocity, $\dot{x}_p(t)$, and, as the output, the damper force $F_d(t)$, with a constant electric field setting $E(t)$.

Remark 3. Considering that the applied electric field is uniform, one has:

$$
E(t) = -\frac{U(t)}{d_e} = -\frac{U_m}{d_e}v \tag{10}
$$

where d_e is the distance between electrodes; U_m is maximum voltage; v is duty cycle of PWM channel.

Substituting (10) into F_{ER} in Equation (9), one obtains:

$$
\begin{aligned}
F_{ER}(t) &= (A_p - A_s)\frac{cL_d}{d}\alpha(-\frac{U_m}{d_e})^{\beta}v^{\beta} \\
&= \sigma v(t)^{\beta}
\end{aligned} \tag{11}
$$

where $\sigma = (A_p - A_s)\frac{cL_d}{d}\alpha(-\frac{U_m}{d_e})^{\beta}$

In Figure 7, some simulation results of the developed static model [1] are seen, given a Force *vs.* Deflection plot and a Force *vs.* Deflection Velocity

[1]The identification procedure of the static model is detailed in Section 4

diagram. In this Figure, it is possible to check that the behavior of the model is close to a real damper's behavior (see Figure 4), but it still does not well represent the behaviour of velocities close to zero; this is a critical case wherein the damper dynamics directly affects the force and will be handled in the next subsection.

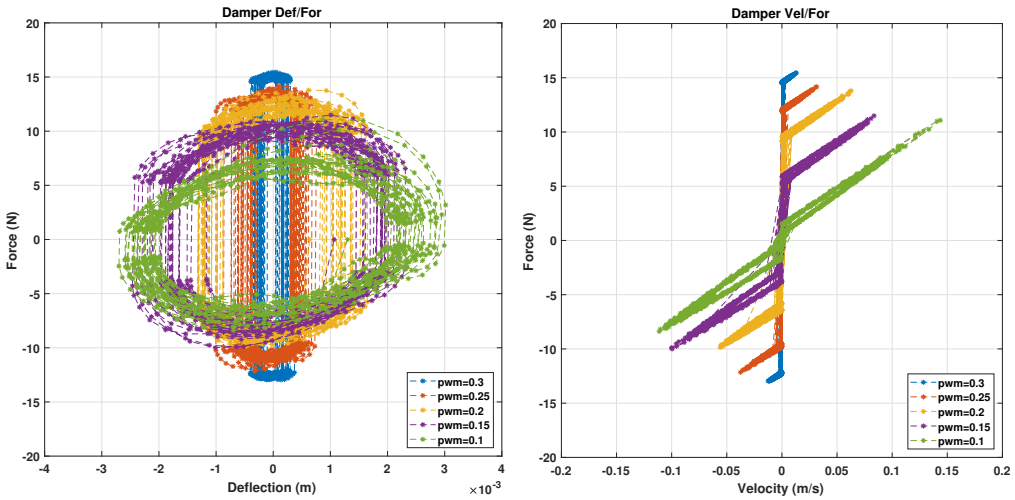

Figure 7: Static Model Simulation

Remark 4. In Figure 7, as expected, the force range has still to be adjusted, as the model parameters haven't yet been properly adjusted.

3.2. Parametrical Dynamic Model of ER *Dampers*

In this subsection, the dynamic modeling of Electro-Rheological dampers is detailed in order to achieve a complete (with static and dynamic parts) control-oriented model of these *ER* automotive shock absorbers.

In the previous subsection, during the static validation procedure, the input used to study these dampers were constant deflection velocity profiles. Now, the procedure followed for a dynamic analysis consists in changing this input to dynamical excitations (such as sinusoidal sources). Then, with collected data from a real testbed, a dynamic model could be found, as it was similarly done in [33], [3], [6] and [18].

Remark 5. In the static conditions, the piston inside the damper chamber, that feeds the internal fluid dynamics, has stationary conditions, whereas for the dynamic case, neither the velocity of the piston nor the fluid flow are constant.

The dynamic behaviour of a system can be studied in time and frequency domains. Herein, a time-wise procedure will be followed but, before entering into further details, it is first beneficial for the reader to become familiar with the characteristics of a dynamical damping curve.

After several empirical tests, it was noted that the dynamics of the *ER* fluid can be approximated accurately enough by a first order system, with a damping time constant T_{d}. This means that the third part of equation (9), related to the force due to the yield stress of the Rheological fluid, will be no longer considered as static, but dynamic, as represented below:

$$T_{\mathrm{d}} \frac{dF_{ER}}{dt}(t) + F_{ER}(t) \quad = \quad \sigma v(t)^{\beta} \tag{12}$$

Then, coupling the static equation (9) with the dynamic law (12) leads to the following, conclusive, parametrical dynamical model of the *ER* damper force:

$$\begin{aligned} F_d(t) \quad &= \quad \overbrace{[P_a(t)A_s]}^{\text{Gas compliance}} \; + \; \overbrace{c_{vis}\dot{x}_p(t)}^{ER\text{ Viscosity}} \\ &+ \quad \underbrace{F_{ER}(t)\mathrm{sign}\{\dot{x}_p(t)\}}_{\text{Yield stress}} \end{aligned} \tag{13}$$

where c_{vis} encompasses the constants $\left(\frac{6\mu L_d}{\pi d^3 R_d}\right)$.

This final dynamic model stands as an accurate behaviour of a real *ER* damper. This is confirmed in Figure 8, where two Force *vs.* Deflection Velocity plots are given, for static and dynamic tests.

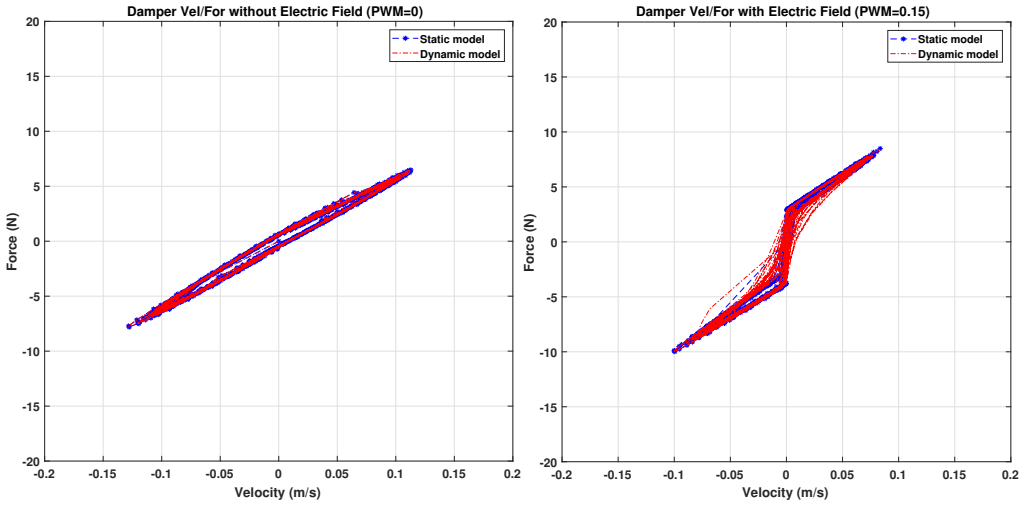

Figure 8: Static Model and Dynamic Model

3.3. Validation Results

Finally, let some validation results be shown, using the final complete Electro-Rheological damper model (13). For this, the study compares the behaviour of this model with the behaviour of a real *ER* damper, considering the use of a real mechatronic test-rig equipped with four semi-active *ER* dampers (refer to Section 2).

For the validation goals, a sinusoidal input deflection velocity is considered, taken at different frequencies for each electric field setting. The velocity input is taken within $[-0.15\,,\,0.15]\,\frac{\mathrm{m}}{\mathrm{s}}$ at frequencies $[0.1\,,\,1000]\,\mathrm{Hz}$ and the PWM signals are taken within $[10\,,\,30]\,\%$. As the used testbed is equipped with deflection and force sensors, one can compare the Force *vs.* Deflection Velocity plot, for different PWM signals (that control the electric field $E(t)$), considering real data and data obtained with the simulation model, see Figure 9, where the behaviours of the real plant and of the proposed *ER* damper model are given.

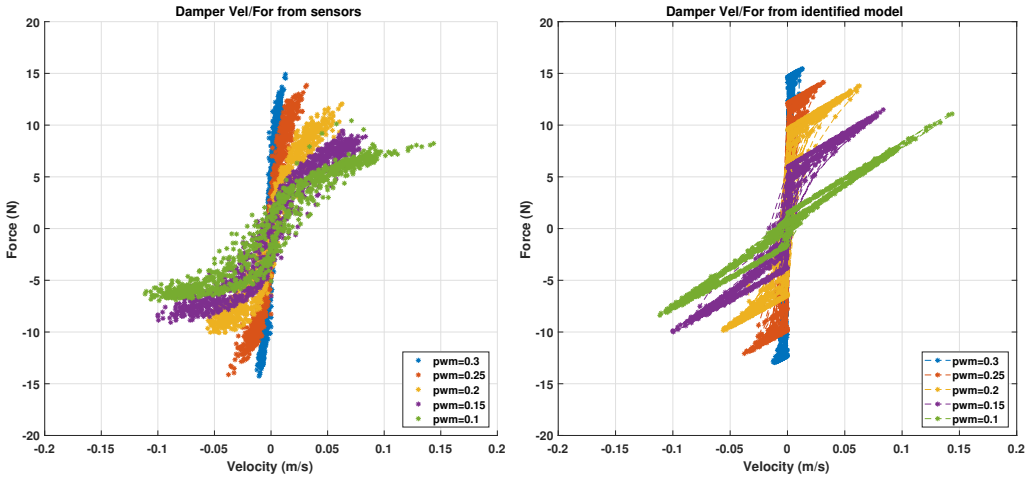

Figure 9: Model Validation: Real Data

By analyzing Figure 9, one can clearly conclude that there exists a good agreement between the real measurements and the simulation of the proposed model. The perfect agreement between curves was achieved with the correct parameters for the used test bench. Their identification is presented in the next Section.

4. Identification procedure of Model Parameters

This Section presents the identification of the model parameters (given in Equations 13 and 12), considering the front-left *ER* damper of the *INOVE Soben-Car* vehicle platform, as explained in Section 2.

Before presenting the actual identification procedure, some considerations have to be made. Around the zero-velocity region, when the movement of the piston changes direction, the damping force values are lower when accelerating than when decelerating - this is the *Hysteresis* phenomenon. A common problem, when dealing with transducers, is the hysteresis error: different force outputs for the same velocity input, depending on the acceleration direction of the piston. Hysteresis is due to energy dissipation sources (such as friction) or to magnetic materials. Therefore, in order to increase the accuracy of the proposed simulation model, the incipient friction of the damper piston must be taken into account so that the hysteresis behaviour

is translated by the achieved dynamical model. The effect of hysteresis in models has been discussed in [29].

As stated, to cope with the incipient hysteresis effect of the damper and in order to increase the accuracy of the proposed model, each parameter of the proposed model will be identified separetely for the release movement and the compression movement. This leads to a model with parameters that vary according to the piston's behaviour: compression or release movement. Doing so, the hysteresis effect is naturally represented, and the energy loss due to the inertia and friction of the piston are taken into account.

Different experimental configurations were carried out to estimate the parameters characterizing the final global model (13). These tests consist in changing the magnitude and the frequency of the external inputs of an *ER* shock absorber (Velocity, Electric Field) in order to identify the critical response of the system. To identify the values, it is necessary to check the damper output (Force) with respect to the inputs (Velocity, Electric Field, *etc*).

The final model 13 and 12 has to be identified and all the conducted identification procedures are explained in the sequel.

4.1. Gas Compliance and ER Viscosity Terms

The first factor involved in the proposed model is the elastic characteristic of the *ER* damper, generated by the presence of the gas chamber inside the system. This factor is related to the force generated by the compression of the gas, and its behavior can be accurately approximated by the behaviour of a spring, as described in Equation (14). This assumption is quite reasonable and coherent with the existent damper models: as stated in [9], k_{nom} represents the effective stiffness of the damper due to the gas pressure.

$$P_a(t)A_s \;\approx\; k_{nom}x_p(t) \tag{14}$$

On the other hand, the second term in Equation (13) represents the damping force due to the natural fluid viscosity of the *ER* damper, in the absence of electric field. It is also important to remark that the identification of the natural viscosity parameter (c_{vis}) has to be done in both positive and negative velocities regions, in order to determinate the difference between release and compression movements.

To identify the parameters (k_{nom}, c_{vis}), the experimental tests consist in submitting the damper to a null control signal ($E(t) = 0$). In this case, the

damper force, when no electric field is applied to the damper, results from the gas compliance and ER fluid viscosity. Thereforce, the damper force is obtained as follows:

$$\begin{aligned} F_d(t) &= k_{nom} x_p(t) + c_{vis} \dot{x}_p(t) \\ &= [x_p(t), \dot{x}_p(t)] \begin{bmatrix} k_{nom} \\ c_{vis} \end{bmatrix} \end{aligned} \tag{15}$$

The parameters k_{nom} and c_{vis} in (15) are identified by the Least Squares Method, see [26], i.e solving

$$\underset{\theta_1}{min} \quad \frac{1}{N} \sum_{i=1}^{N} (y_{1i} - x_{1i}\theta_1)^2 \tag{16}$$

where $\theta_1 = \begin{bmatrix} k_{nom} \\ c_{vis} \end{bmatrix}$, y_{1i} is the measured damper force, x_{1i} are the sensors measurements ($x_p(t)$, $\dot{x}_p(t)$).

The identified parameters k_{nom} and c_{vis} are given in Table 2.

4.2. Yield Stress Term

The second part to be identified contains the parameters related to the force due to the yield stress of the *ER* fluid, which can be continuously controlled by the intensity of the electric field applied to the damper. During this experiment, the damper undergoes a sinusoidal deflection with different electric fields. Indeed the force provided by the damper at a given deflection velocity can be controlled by changing the input voltage ($U(t)$, controlled by a *PWM* signal) of the *ER* damper. Therefore, once the parameters k_{nom} and c_{vis} are determined, the last parameters to be identified of the achieved damper force law are α and β. They are related with the effect of the control signal (electric field, $E(t)$) upon the damper's behavior.

Considering the used testbed, the relationship between a controlled *PWM* signal and the voltage applied to the damper is shown in the Table 1; see Equation (10) for the relationship between applied tension and electric field. Then, the yield stress parameters α and β in Equations (7) and (12), can be identified by analyzing the damper force, at the same piston velocity profile, with different applied Electric fields. The experimental tests considered the

velocity input within the range $[-0.15\,,\,0.15]\,\frac{\mathrm{m}}{\mathrm{s}}$ and an the PWM signals varying inside the set $[0\,,\,30]\,\%$.

The parameters σ and β are estimated using a Nonlinear Least Squares Method [28], considering the force values for different PWM signals ($v = 0.1 \div 0.45$). Based on the identified parameters k_{nom} and c_{vis} from the previous procedure, the force due to yield stress is calculated as follows:

$$F_{YS}(t) = F_d(t) - k_{nom}x_p(t) - c_{vis}\dot{x}_p(t) \tag{17}$$

where $F_{YS}(t)$ represents only the portion of the damper force due to yield stress of the ER fluid.

$F_{YS}(t)$ can be straightforward rewritten as:

$$\begin{aligned} F_{YS}(t) &= \sigma v(t)^{\beta} sign(\dot{x}_p(t)) \\ &= \begin{cases} \sigma v(t)^{\beta} & \dot{x}_p(t) > 0 \\ 0 & \dot{x}_p(t) = 0 \\ -\sigma v(t)^{\beta} & \dot{x}_p(t) < 0 \end{cases} \end{aligned} \tag{18}$$

The parameters δ and β are estimated using a Nonlinear Least Squares Method with the cost function given by:

$$J = \underset{\theta_2}{min} \quad \sum_{i=1}^{N} (y_{2i} - f_{2i}(x_{2i}, \theta_2))^2 \tag{19}$$

where the vector θ_2 contains the parameters (σ, β), y_{2i} is the measurement data of $F_{YS}(t)$, considering Equation (17), $f_{2i}(x_{2i}, \theta_2)$ represents the force from yield stress in Equation (18), x_{2i} are the duty cycle of PWM channel ($v(t)$) and piston's velocity ($\dot{x}_p(t)$), available measurements from the testbed.

The identified paramenters σ, β are given in Table 2.

Figure 10 shows a comparison between the real controlled force $F_{ER}(t)$ (given by force sensors) and the model-based $F_{ER}(t)$, with the adjusted parameters σ (see Equation (11)) and β, for different PWM signal values.

Table 1: Relationship: PWM and Applied Tension

PWM Signal	$U(t)$
0 %	0 kV
20 %	1 kV
40 %	2 kV
60 %	3 kV
80 %	4 kV
100 %	5 kV

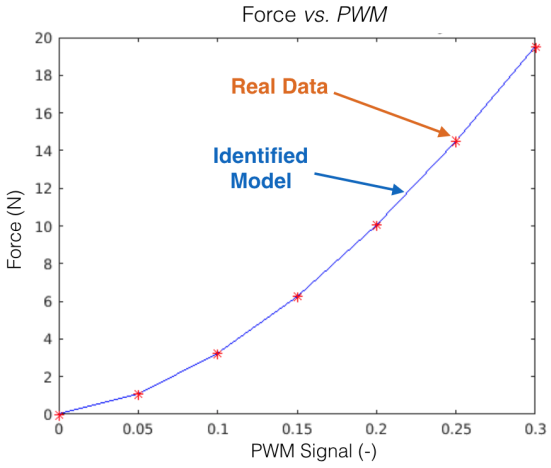

Figure 10: Model Parameter Identification: Yield Stress Parameters

Table 2: Identified ER Damper Parameters

Parameters	Value		Unit
	Compression	Release	
k_{nom}	263.1168	170.4045	N/m
c_{vis}	64.6433	68.8289	N.s/m^2
T_{d}	43	43	ms
σ	12.8157	17.0442	–
β	0.2373	0.3948	–

4.3. Final Validation

4.3.1. Case 1

Now, the final validation results of the proposed Electro-Rheological damper model are presented, considering the adjusted identified parameters for the *INOVE Soben-Car* mechatronic test-rig. The new adjusted Force *vs.* Deflection and Force *vs.* Deflection Velocity diagrams are given, respectively, in Figures 11 and (previously presented) 9, comparing the proposed damper model and real data measured from available sensors on the platform.

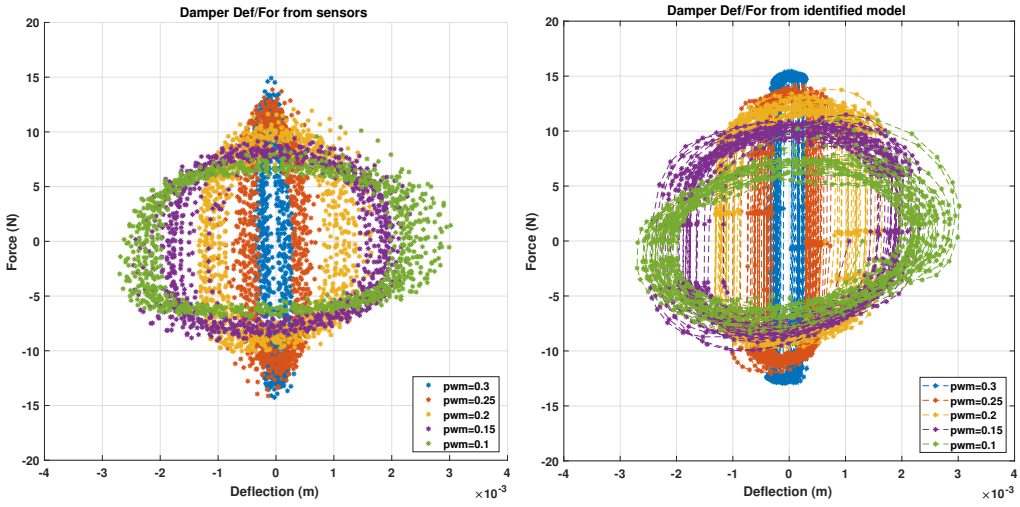

Figure 11: Final Model Validation Results: Force *vs.* Deflection (Case 1)

4.3.2. Case 2

Considering the road profile of a vehicle running at 120 km/h in a straight line on a dry road, when it encounters a sequence of 10 mm sinusoidal bumps, the results comparing the model-based computed force and the real (measured) force are given by Figures 12 and 13. Clearly, the model is well adjusted.

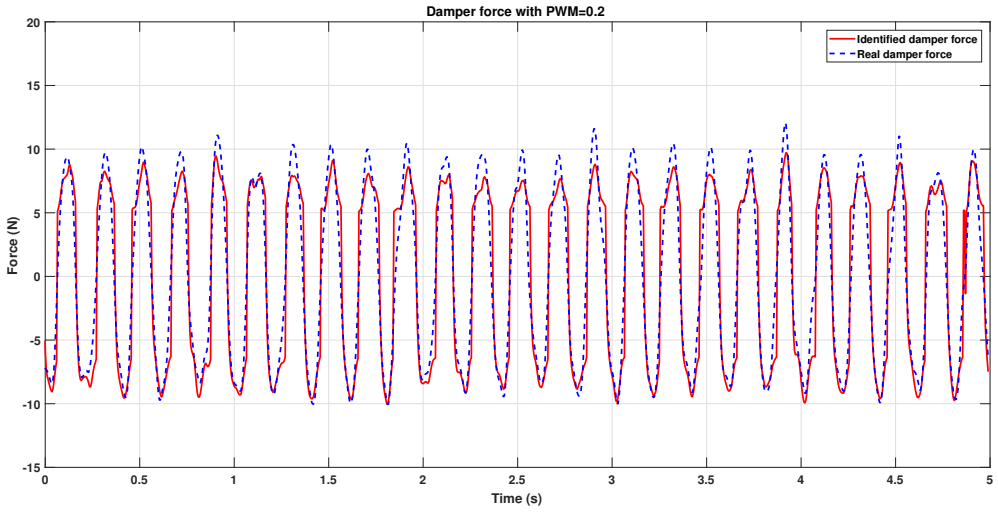

Figure 12: Validation Results: Model-based and Real Force - Sinusoidal Road Profile (Case 2)

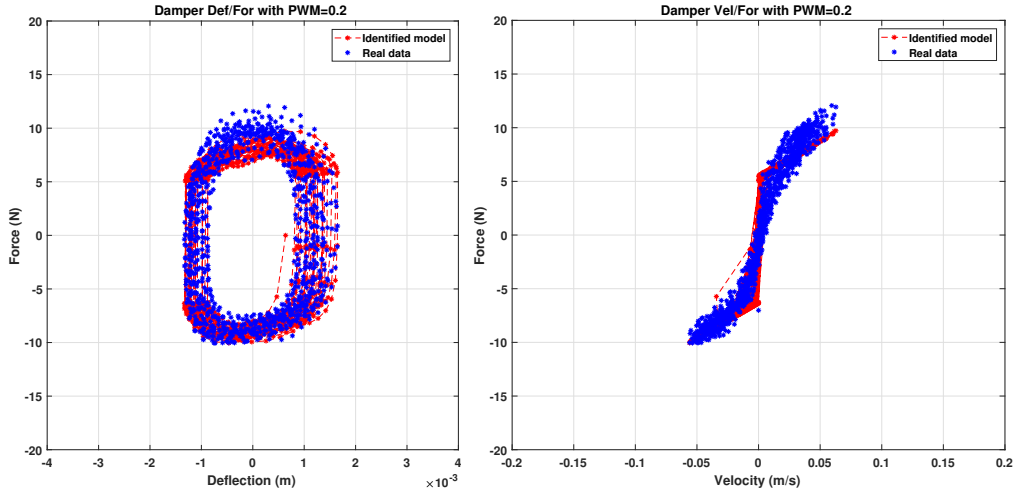

Figure 13: Validation Results: Damper Diagrams - Sinusoidal Road Profile (Case 2)

The proposed model is now **very** accurate and describes very well the dynamics of an Electro-Rheological damper, which is one of the main goals

of this article. To further illustrate this accurateness, Table 3 presents the normalized root-mean-square errors, considering the difference between the adjusted model force and real measured force, for different PWM values.

Table 3: Final Validation: Normalized Root-Mean-Square Errors

PWM Signal	$NRMSE$
10 %	0.0685
15 %	0.0682
20 %	0.0997
25 %	0.1664
30 %	0.1883

5. Fault Modelling for *ER* Dampers

This Section deals with the second main contribution of this paper i.e. the issue of fault modelling for Electro-Rheological dampers. The objective herein is to develop accurate models that take into account the effect of different kinds of faults upon the force response of *ER* dampers.

Herein, the most common types of faults affecting *ER* dampers are analysed, together with their effects upon the force delivered by the damper. These faults are split into four distinctive kinds: electric faults, physical deformation faults, oil leakage faults and faults due to high temperatures. Each kind of fault will be analysed by one of the subsection below.

5.1. Oil Leakage Faults

As described repeatedly throughout this work, the *ER* damper can be defined as an advanced shock absorber. In the case of shock absorbers, the most common faults are oil leakages. Due to several reasons, such as the high pressures inside the system or simply an impact, the system may present a loss on the quantity of its damping fluid. This situation directly affects the global behavior of the shock absorber.

This kind of oil leakage fault is of most interest to the scientific community for an accurate modelling of this phenomenon. If the amount of damping fluid decreases, the flow inside the damper chamber also decreases, which implies a loss of effectiveness of the damper's force. In order to represent this kind

of fault, the loss of effectiveness factor can be taken as inversely proportional to the fluid flow.

Regarding the faulty Electro-Rheological damper situation, these faults can be considered as of multiplicative form upon the force produced by the damper. considering *loss of effectiveness* factors, as proposed in [20]. These factors are assumed to be constant or slow-varying and can represent anything that leads to a loss in the effectiveness of the damper, for instance, an oil leakage, physical deformation or even the presence of air inside the *ER* fluid duct.

The loss of effectiveness factor $f_1(t)$ is bounded inside the set $[0\ ,\ 1]$, where $f_1(t) = 1$ means that the system is faultless and $f_1(t) = 0$ means that all the *ER* fluid has leaked from the damper chamber. To simulate this fault, this factor $f_1(t)$ has to be incorporated in to the proposed *ER* damper model (13), as follows:

$$\begin{aligned} F_d(t) &= f_1(t)[P_a(t)A_s + c_{vis}\dot{x}_p(t) \\ &+ F_{ER}(t)\text{sign}\{\dot{x}_p(t)\}] \end{aligned} \tag{20}$$

$$f_1(t) \propto \frac{1}{Q_d(t)} = \frac{1}{\dot{x}_p(t)} \tag{21}$$

This fault affects directly all the force computed by the proposed model (except friction and inertial force, mostly related to hysteresis). In other words, this fault affects the controllable and the nominal behavior of the *ER* damper. In terms of simulation, two results are presented in Figure 14, with leakage faults of 50 % of the *ER* fluid, with and without an electric field.

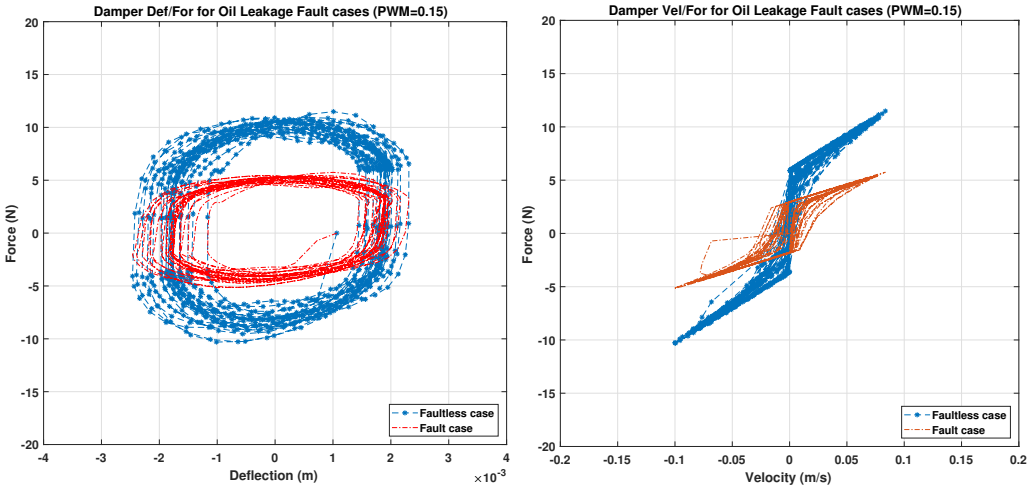

Figure 14: Oil Leakage Fault Simulation: 50 %

5.2. Electrical Fault

The difference between Magneto-Rheological and Electro-Rheological dampers consists, mainly, in what actually acts upon the controllable part of the damping force. For the first kind, the control source is given by a magnetic field, whereas for the latter, it is given by an electric field. The electronic circuit used to obtain the desired electric field is much more complex than the one used to sustain a magnetic field. Indeed, in order to obtain the magnetic field, it is necessary to work with power in the order of magnitude of V, whereas for the electric field it is usually necessary to work in the order of kV.

Therefore, the crucial circuit must be considered as a second potential source of faults in the *ER* damper system. The effect of this kind of fault, in comparison to the oil leakage fault, is that it varies only the yield stress term - i.e. the controllable part of the damping force $F_d(t)$. Suppose that the circuit sustaining the electric field completely fails, then the yield stress in Equation (13) becomes null.

For this reason, the loss of effectiveness fault factor $f_2(t)$ is set only upon $F_{ER}(t)$, as depicts Equation (22). This fault factor $f_2(t)$ can be computed as proportional to the loss upon the electric field, in terms of the electronic failures on the circuit responsible for providing $E(t)$, whereas these instrumentation details will not be investigated herein.

$$
\begin{aligned}
F_d(t) &= P_a(t)A_s + c_{vis}\dot{x}_p(t) \\
&+ f_2(t)F_{ER}(t)\text{sign}(\dot{x}_p(t))
\end{aligned} \tag{22}
$$

Some simulation responses of this kind of fault are shown in Figure 15. Remark that, once again, $f_2(t)$ is bounded inside the interval $[0\ ,\ 1]$, where $f_2(t) = 0$ represents a complete electrical circuit crash.

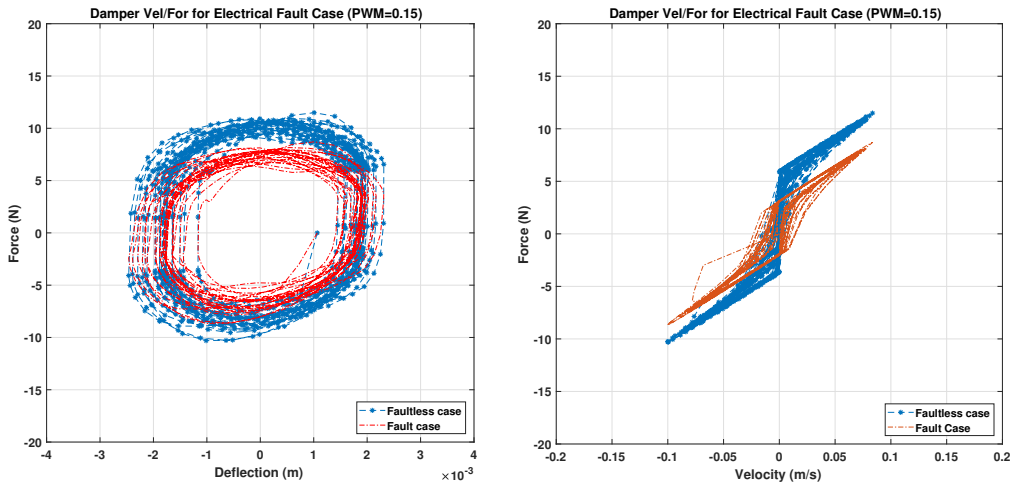

Figure 15: Electrical Fault Simulation: 50 % of Loss on $E(t)$

5.3. Physical Deformation Faults

In terms of physical faults, it is important to state that most industrial manufacturers of *ER* dampers have recently decided to add some spirals to the inner ducts of these dampers, in order to increase the path that the fluid must travel and thus to enlarge the damping effect. As the fluid has a longer path to travel, the force given by the damper increases, but the pressure inside the fluid chamber also increases. This higher pressure present in newer *ER* dampers has also to be considered as a third potential source of faults, since it might cause a physical deformation of the inner path of the fluid. Figure 16 shows an inner duct of a real *ER* shock absorber, from *SOBEN* (see `www.soben.fr`).

Figure 16: Spirals of the inner electrode of an *ER* Damper - Faultless (left) and Faulty (right)

This fault directly affects the length of the annular duct. Note that this parameter is related both to the controllable force and the nominal damping factor. Thus, this fault can be expressed as in Equation (23), where $f_3(t)$ is the loss of effectiveness fault factor for physical deformation faults.

$$\begin{aligned} F_d(t) &= [P_a(t)A_s] + f_3(t)[c_{vis}\dot{x}_p(t) \\ &+ F_{ER}(t)\text{sign}\{\dot{x}_p(t)\}] \end{aligned} \tag{23}$$

Some simulation responses of this type of fault are shown in Figure 17, where physical faults of 50 %, with and without the presence of an electric field. Remark that, once again, $f_3(t)$ is bounded inside the interval $[0\ ,\ 1]$, where $f_3(t) = 0$ represents a very strong deformation such that the *ER* can no longer flow through the inner duct.

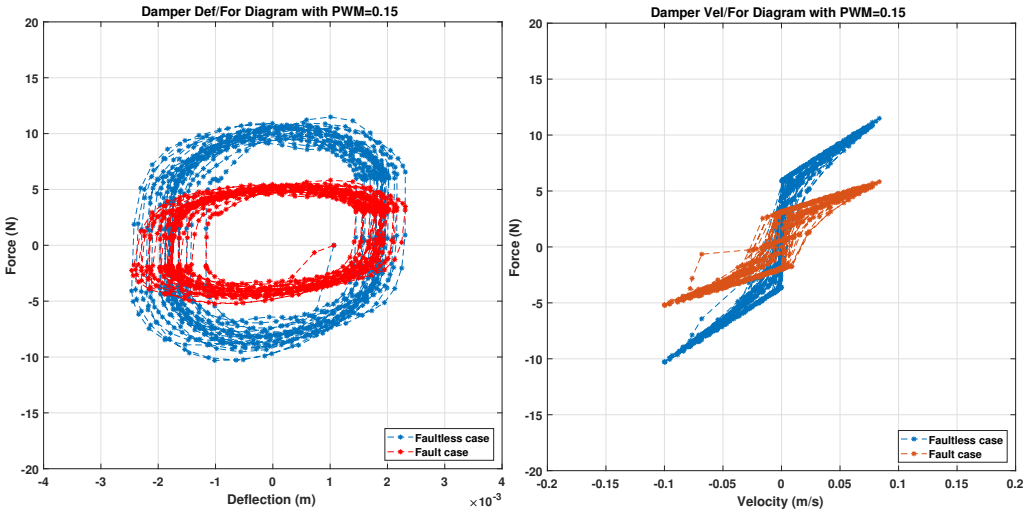

Figure 17: Physical Deformation Fault Simulation: 50 %

5.4. High Temperature Faults

Finally, the last potential source of failures that has to be considered for a full fault analysis of *ER* dampers is the working temperature of the Electro-Rheological fluid. In the industrial assembly process of a shock absorber, external particles, such as air or dirt, may enter the fluid chamber. These particles might lead to potential failure: as the *ER* dampers work with high voltage sources, when they are in contact with the electric field, their temperature can potentially increase and burn the shock absorber from the inside out. In practice, this fault destroys the damper and, for this reason, this kind of failure will not be considered in this work. The only solution to this problem is to monitor the temperature of the damper and stop its operation if it reaches a very high value (over 60 or 70 ° C), as done in the testbed.

Remark 6. An analysis of the temperature's effect upon the force made by *ER* damper is done in [34]. This characteristic was neglected in the modelling section of this work, considering that the use of *ER* dampers in semi-active suspension systems usually operate with the *ER* fluid within a rather constant temperature set. It has been observed in [32], nonetheless, that over 50 ° C the *ER* fluid's shear stresses no longer increase, due to enlarging the applied electric field. Anyhow, in most *ER* dampers, specially those in the used test

rig [45], there are temperature monitoring systems that prevent the fluid's temperature to increase to yield problematic situations.

5.5. Illustration of the fault cases

Finally, a complete illustration between the faults due to electrical failures, physical deformation and oil leakage is presented below, in Figure 18.

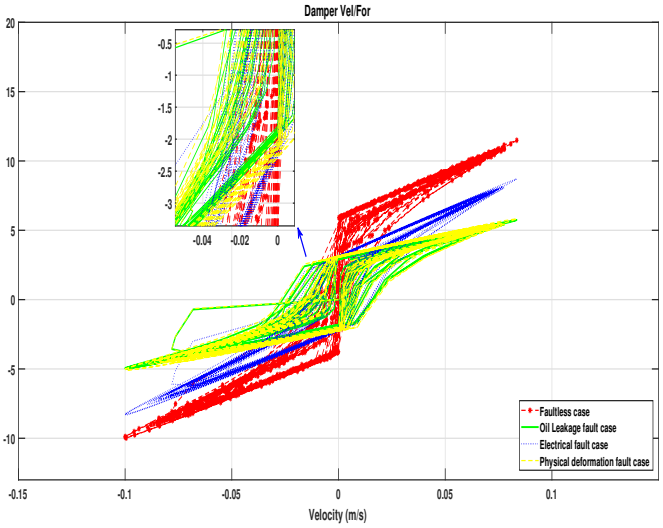

Figure 18: Different Faults Simulation

6. Fault Experimental Emulation in Real *ER* Dampers

Throughout literature, it is possible to find some experimental testbeds that allow the user to simulate faults inside shock absorbers, as in [20], where a special valve was added to a regular damper to simulate faults by adding or subtracting fluid inside the damper. This approach presents some good results, but it might be costly. The *ER* dampers used in the experimental platform of this work have been solely designed and made for the considered scaled vehicle, see [44], and an additional valve is not a conceivable solution.

Then, how can faults be experimentally emulated in a real vehicle test-rig without adding new components? It is proposed here to use the controllable part of the damper force so that the total force $F_d(t)$ mimics a real faulty situation what is refered to as fault emulation

Depending on the desired kind of fault to be emulated, one can compute the control PWM signal $v(t)$ so that the actual damper force output $F_d(t)$

is seemingly faulty. This method was tested first in simulation and after a good overall representation of faults, it was tested on the real platform (see Section 2). Thus, the method for experimental implementation of faults are here presented and the results retrieved from the *INOVE Soben-Car* are shown, considering oil leakage, electrical and physical deformation faults. In experimental tests, the duty cycle of PWM $v = 0.3$ is chosen for healthy case while the road profile is a sequence of sinusoidal bumps, see Figure 19

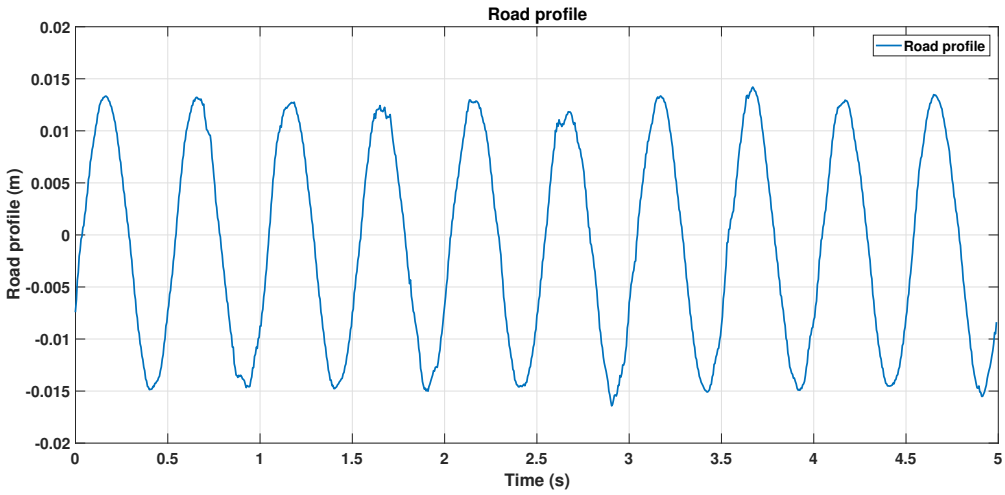

Figure 19: Road profile

6.1. Oil Leakage Fault

To mimic a faulty situation, it is necessary to find a PWM signal for oil leakage fault case v_{f_1} from measurement data (x_p, $\dot{x}_p$ are shown in Figure 20 and Figure 21) of healthy case with PWM signal $v = 0.3$. The control input signal v_{f1} is then applied to the real ER damper in the INOVE testbed. As a result, the corresponding force made by the damper $F_d^{f_1}$ is seemingly faulty.

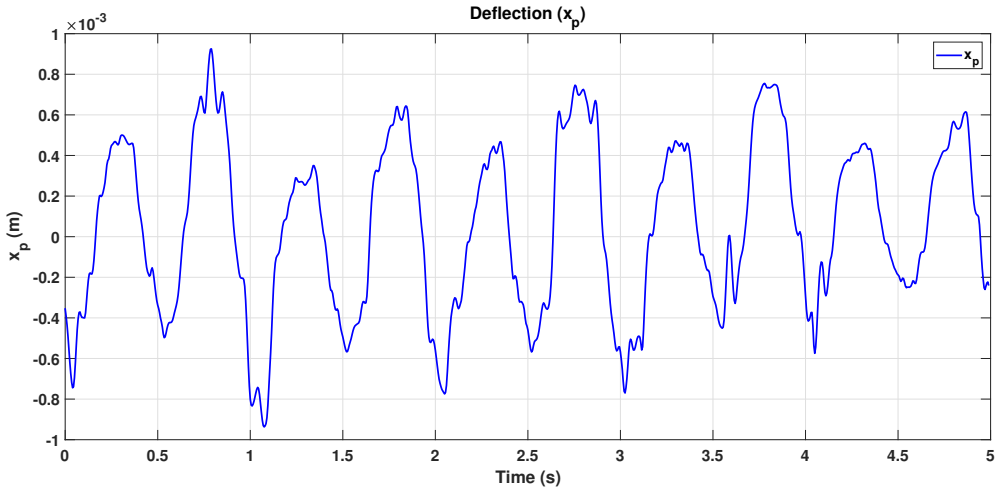

Figure 20: Measured Deflection

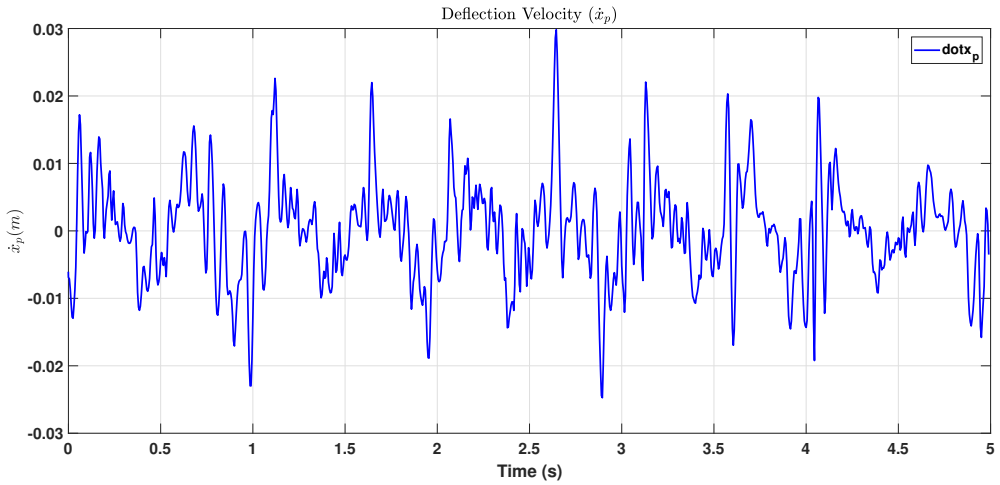

Figure 21: Deflection Velocity

The Equation (20) that represents oil leakage faults in *ER* dampers is recalled

$$F_d^{f_1} = f_1[k_{nom}x_p + c_{vis}\dot{x}_p + F_{ER}\text{sign}(\dot{x}_p)] \tag{24}$$

where f_1 represents the desired loss of effectiveness fault due to oil leakage.

In order to implement the oil leakage fault in semi-active damper, the damper force that mimics the damper oil leakage is given by

$$F_d^{mimicf_1} = k_{nom}x_p + c_{vis}\dot{x}_p + F_{ER}^{f_1}\text{sign}(\dot{x}_p) \tag{25}$$

From (24) and (25), $F_{ER}^{f_1}$ is obtained such that $F_d^{f_1} = F_d^{mimicf_1}$

$$\begin{aligned} F_{ER}^{f_1} &= (f_1 - 1)(k_{nom}x_p + c_{vis}\dot{x}_p)\text{sign}(\dot{x}_p) \\ &\quad + f_1 F_{ER} \end{aligned} \tag{26}$$

A fault-mimic PWM signal v_{f_1} can be then calculated as follows:

$$v_{f_1} = \left[\frac{(f_1 - 1)}{\delta}(k_{nom}x_p + c_{vis}\dot{x}_p)\text{sign}(\dot{x}_p) + f_1 v^{\beta}\right]^{\frac{1}{\beta}} \tag{27}$$

In experimental test, the oil leakage fault factor f_1 is chosen as 50%. Based on measurement data (x_p, $\dot{x}_p$) and PWM signal of healthy case $v = 0.3$, the duty cycle of PWM signal (v_{f1}) is calculated using equation (27), shown in Figure 22. Figure 23 shows a Force *vs.* Piston velocity diagram, considering model-based and real data responses for the faulty and healthy situations.

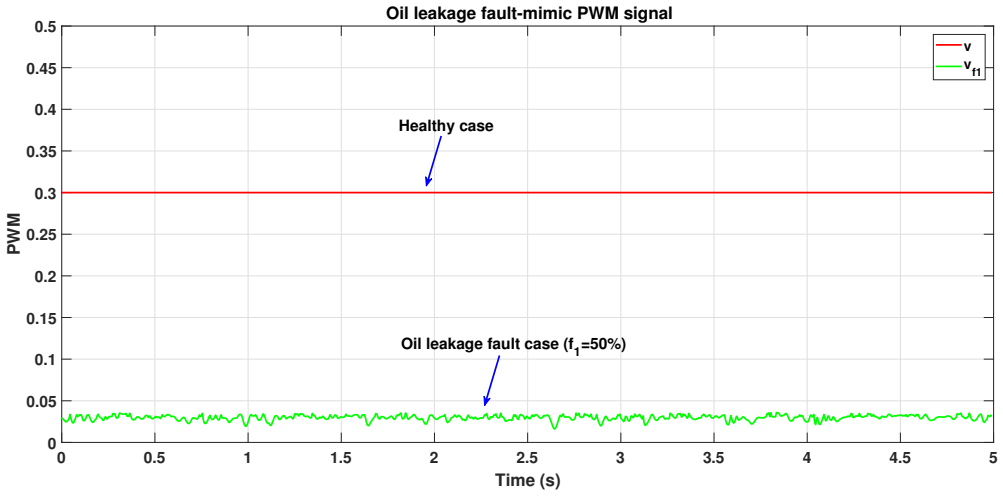

Figure 22: Oil leakage fault-mimic PWM signal

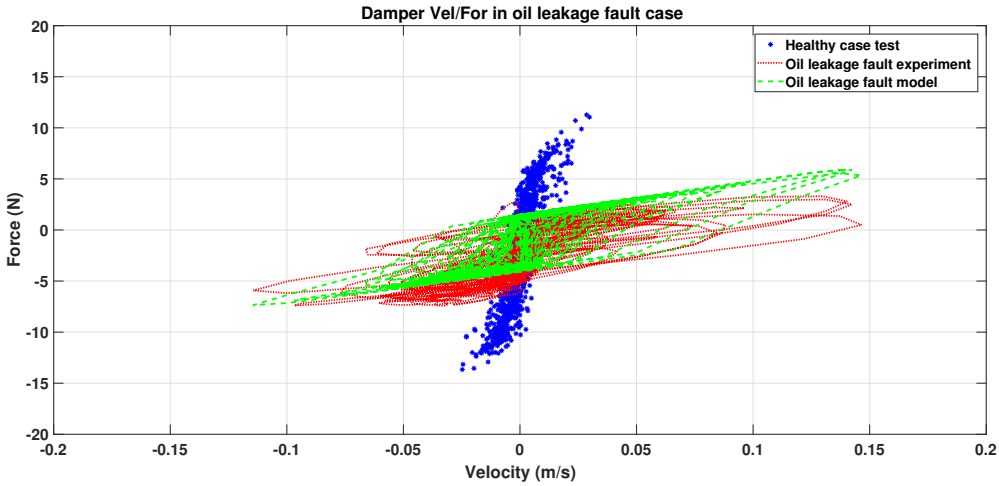

Figure 23: Effect of the oil leakage fault in the Force vs. Velocity characteristic diagram.

6.2. Electrical Fault

Similarly to mimicking the oil leakage fault in section 6.1, the duty cycle of PWM channel v_{f_2}, used to implement electrical fault case, is calculated based on the measured data of faultless case with control input v. The steps to find v_{f_2} are as follows

First, the Equation (22) is rewritten

$$F_d^{f_2} = k_{nom}x_p + c_{vis}\dot{x}_p + f_2 F_{ER}\text{sign}(\dot{x}_p) \tag{28}$$

where f_2 represents the desired loss of effectiveness fault due to electric.

Second, the corresponding damper force mimicking the electrical fault is defined as follows

$$F_d^{mimicf_2} = k_{nom}x_p + c_{vis}\dot{x}_p + F_{ER}^{f_2}\text{sign}(\dot{x}_p) \tag{29}$$

From (28) and (29), it is easy to obtain $F_{ER}^{f_2}$

$$F_{ER}^{f_2} = f_2 F_{ER} \tag{30}$$

In this case, the PWM signal v_{f_2} to simulate the electrical fault is obtainedv as

$$v_{f_2} = f_2^{\frac{1}{\beta}} v \tag{31}$$

In order to calculated v_{f_2} for real test, the desired electrical fault (f_2) and PWM signal of healthy case (v) are chosen 50 % and 0.3, respectively. Then the PWM signal for electrical fault case is computed by using Equation (31), shown in Figure 24 . The effect of electrical fault on the Force vs. Velocity characteristic diagram in comparison with the health and fault cases is shown in Figure 25

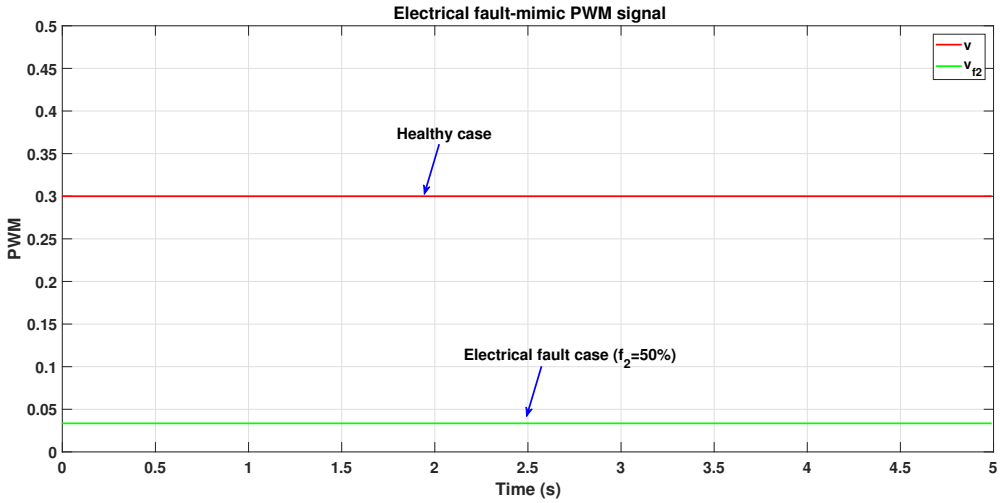

Figure 24: Electrical fault-mimic PWM signal.

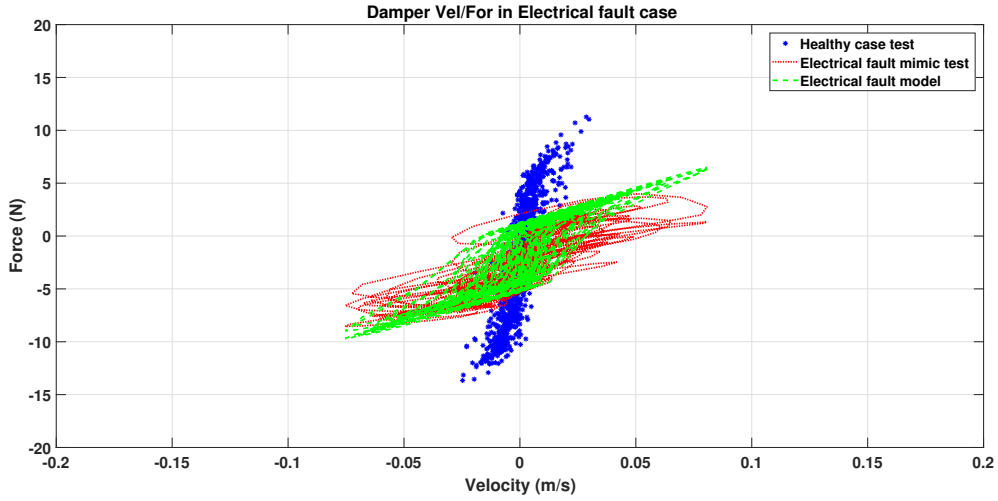

Figure 25: Effect of the electrical fault in the Force vs. Velocity characteristic diagram.

6.3. Physical Deformation Fault

In order to simulate experimentally the physical deformation fault in real testbed, the procedure to find the corresponding PWM signal for this fault v_{f_3} is similar to the ones in section (6.1) and (6.2)

The physical deformation fault in ER damper is presented in the Equation (23)

$$F_d^{f_3} = k_{nom}x_p + f_3\left[c_{vis}\dot{x}_p + F_{ER}\text{sign}(\dot{x}_p)\right] \tag{32}$$

where f_3 represents the desired loss of effectiveness fault due to physical deformation.

The damper force in the physical deformation fault case can be writen:

$$F_d^{mimicf_3} = k_{nom}x_p + c_{vis}\dot{x}_p + F_{ER}^{f_3}\text{sign}(\dot{x}_p) \tag{33}$$

From (32) and (33), $F_{ER}^{f_3}$ is calculated such that $F_d^{f_3} = F_d^{mimicf_3}$

$$F_{ER}^{f_3} = (f_3 - 1)c_{vis}\dot{x}_p\text{sign}(\dot{x}_p) + f_3F_{ER} \tag{34}$$

The PWM signal v_{f_3}, used to simulate the physical deformation fault in the ER damper, is obtained as follows

$$v_{f_3} = \left[\frac{(f_3 - 1)}{\delta} c_{vis} |\dot{x}_p| + f_3 v^{\beta} \right]^{\frac{1}{\beta}} \tag{35}$$

The fault-mimic PWM signal (v_{f_3}) is computed by Equation (35) with $f_3 = 50\%$ and $v = 0.3$, shown in Figure 26. The Force vs. Velocity diagram in comparison with the health and fault cases is shown in Figure 27

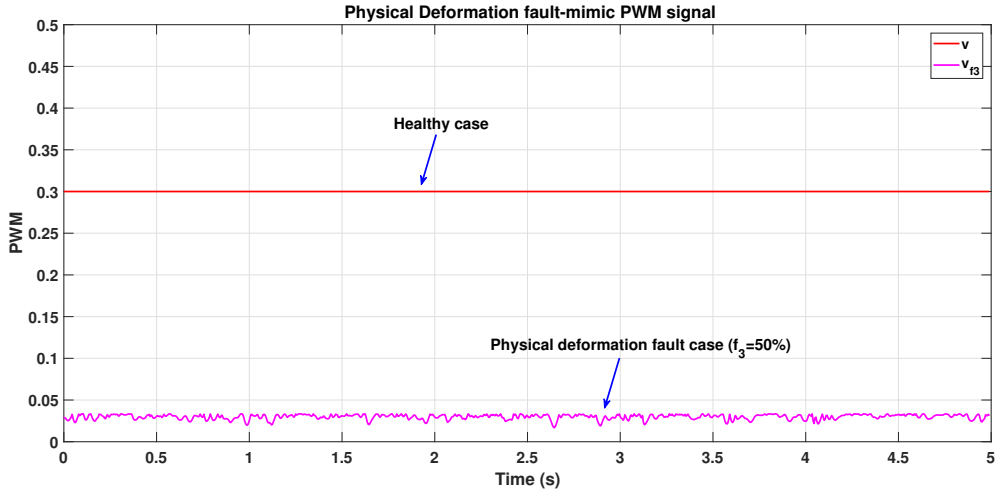

Figure 26: Physical deformation fault-mimic PWM signal.

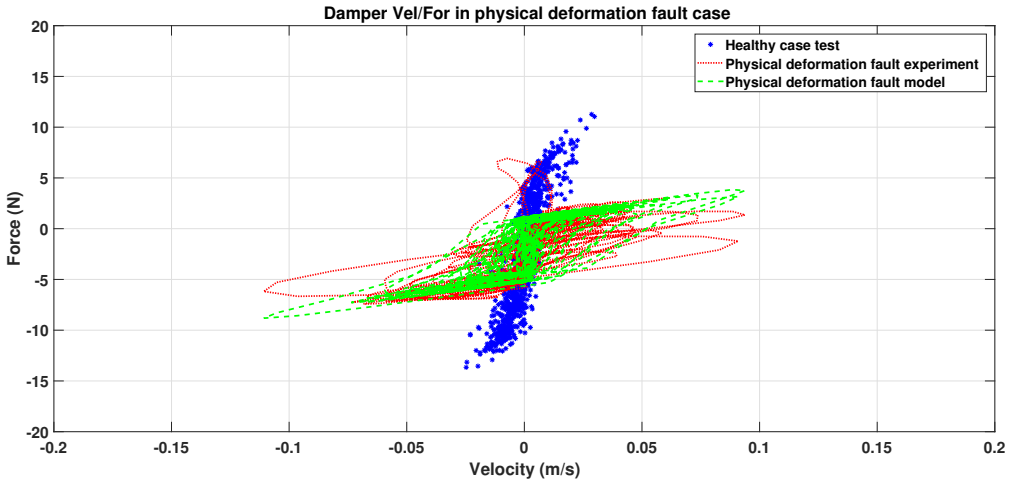

Figure 27: Effect of the physical deformation fault in the Force vs. Velocity characteristic diagram.

6.4. Illustration of the fault cases in a full test

In order to compare the effect of all faults on the damper force, the final test scenario is designed with faults occurring sequentially during the test. The fault-mimic PWM signal is shown in Figure 28. This is of most importance as it is a good proof of the efficiency, reliability and feasibility of the proposed fault simulation method.

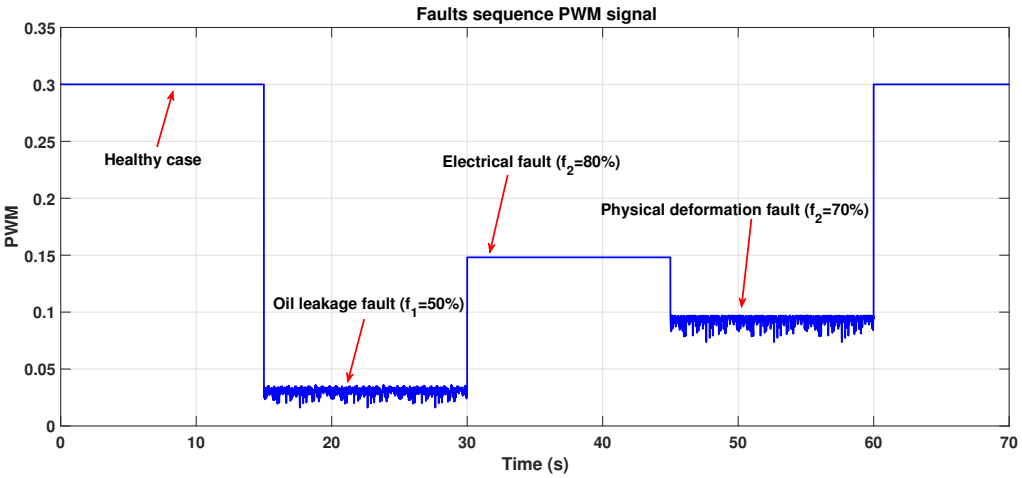

Figure 28: Sequence of fault-mimic PWM signal.

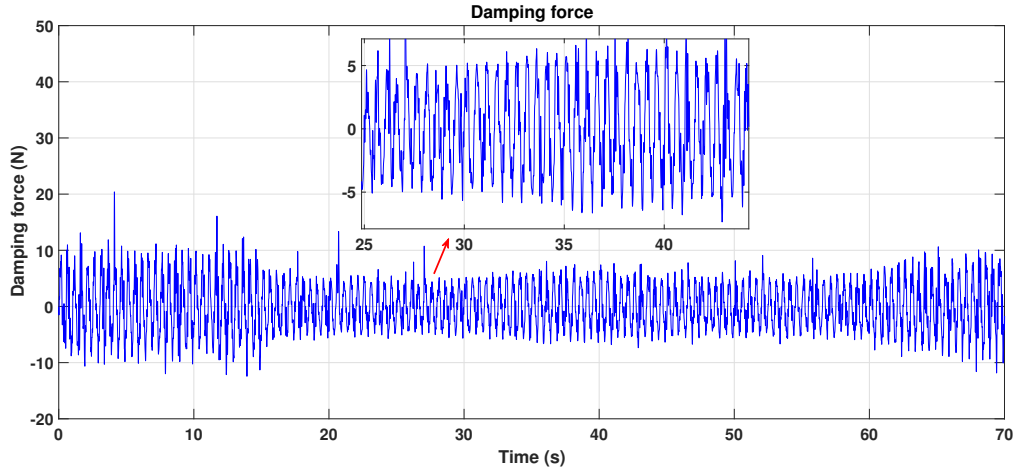

Figure 29: Damping force.

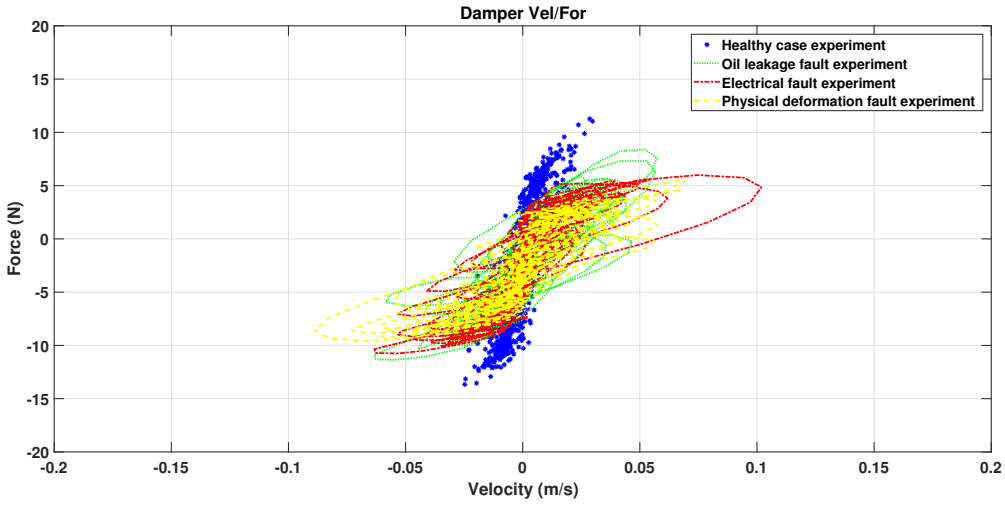

Figure 30: Force vs. Velocity of fault experiments.

Notice how the damper force decreases at $t = 15\,\mathrm{s}$. This is due to a mimicked oil leakage fault. This means that v_{f1} is computed with equation (27), considering a desired fault f_1 as a step to $50\,\%$ at this given instant. During $t = 31\mathrm{s} \div 45\mathrm{s}$, the electrical fault occurs to the damper with the fault factor $f_2 = 80\%$. Then, the mimicked physical deformation fault is simulated from $t = 46\mathrm{s}$ to $t = 60\mathrm{s}$ with $f_3 = 70\%$. The effect of faults on the damper force is shown in the Figure 29. Figure 30 shows a Force *vs.* Piston velocity diagram, considering real data responses for the faulty and faultless situations.

7. Conclusions

This paper presented a thorough analysis of Electro-Rheological Dampers, considering their use for Semi-Active Automotive Suspension Systems. A conclusive parametric dynamical model was presented in terms of an *ER* damper's force; this model was validated with various tests on an experimental platform (reduced vehicle model). Also, the analysis of possible faults that might occur upon these dampers was made, considering how to model the faults and how to experimentally mimic them without adding new components to the test rig.

This is of great interest for designing fault diagnosis and fault tolerant control approach for the automotive suspension systems.

For future works, the authors plan to use the obtained damper force model to develop more accurate control techniques of suspension systems with *ER* dampers and, also, to propose new approaches towards fault detection schemes for these dampers.

Acknowledgements

This work has been partially supported by the *LabEx PERSYVAL-Lab* ($ANR-11-LABX-0025-01$), funded by the French program *Investissements d'Avenir*. The authors also thank *CAPES* for financing project *BRAFITEC ECoSud*.

References

[1] Ashfak, A., Rasheed, K. A., Jaleel, J. A., 2013. Modeling, simulation and experimental validation of magneto-rheological damper. In: International Conference on Advanced Nanomaterials and Emerging Engineering Technologies. IEEE, pp. 267–274.

[2] Aubouet, S., 2010. Modélisation et commande de suspensions semi-actives soben. Ph.D. thesis.

[3] Bhise, A. R., Desai, R. G., Yerrawar, M. R., Mitra, A., Arakerimath, R., 2016. Comparison between passive and semi-active suspension system using matlab/simulink. Journal of Mechanical and Civil Engineering 12, 1–6.

[4] Bingham, E. C., 1929. Rheology. i. the nature of fluid flow. Journal of Chemical Education 6 (6), 1113.

[5] Bird, R. B., Dai, G., Yarusso, B. J., 1983. The rheology and flow of viscoplastic materials. Reviews in Chemical Engineering 1 (1), 1–70.

[6] Bonnecaze, R., Brady, J., 1992. Dynamic simulation of an electrorheological fluid. The Journal of chemical physics 96 (3), 2183–2202.

[7] Choi, S., Choi, Y., Chang, E., Han, S., Kim, C., 1998. Control characteristics of a continuously variable er damper. Mechatronics 8 (2), 143–161.

[8] Choi, S., Lee, H., Chang, E., 2001. Field test results of a semi-active ER suspension system associated with skyhook controller. Mechatronics 11 (3), 345–353.

[9] Choi, S.-B., Han, S.-S., 2003. h_∞ control of electrorheological suspension system subjected to parameter uncertainties. Mechatronics 13 (7), 639–657.

[10] Choi, S.-B., Han, Y.-M., 2007. Vibration control of electrorheological seat suspension with human-body model using sliding mode control. Journal of Sound and Vibration 303 (1-2), 391–404.

[11] Choi, S.-B., Lee, S.-K., Park, Y.-P., 2001. A hysteresis model for the field-dependent damping force of a magnetorheological damper. Journal of sound and vibration 245 (2), 375–383.

[12] de J Lozoya-Santos, J., Morales-Menendez, R., Ramirez-Mendoza, R., Tudon-Martinez, J. C., Sename, O., Dugard, L., 2012. Magnetorheological damperan experimental study. Journal of Intelligent Material Systems and Structures 23 (11), 1213–1232.

[13] Dominy, J., Bulman, D., 1985. An active suspension for a formula one grand prix racing car. Journal of dynamic systems, measurement, and control 107 (1), 73–79.

[14] Dyke, S., Spencer Jr, B., Sain, M., Carlson, J., 1996. Modeling and control of magnetorheological dampers for seismic response reduction. Smart materials and structures 5 (5), 565.

[15] Ehrgott, R., Masri, S., 1994. Structural control applications of an electrorheological device. In: Proc., Int. Workshop on Struct. Control, USC Publ. No. CE-9311. pp. 115–129.

[16] Gamota, D., Filisko, F., 1991. Dynamic mechanical studies of electrorheological materials: moderate frequencies. Journal of rheology 35 (3), 399–425.

[17] Gaul, L., Nitsche, R., 2000. Friction control for vibration suppression. Mechanical Systems and Signal Processing 14 (2), 139–150.

[18] Gavin, H. P., 2001. Multi-duct er dampers. Journal of Intelligent Material Systems and Structures 12 (5), 353–366.

[19] Gillespie, T. D., 1997. Vehicle dynamics. Warren dale.

[20] Hernández-Alcántara, D., Tudón-Martínez, J. C., Amézquita-Brooks, L., Vivas-López, C. A., Morales-Menéndez, R., 2016. Modeling, diagnosis and estimation of actuator faults in vehicle suspensions. Control Engineering Practice 49, 173–186.

[21] Jordan, T. C., Shaw, M. T., 1989. Electrorheology. IEEE Transactions on Electrical Insulation 24 (5), 849–878.

[22] Kakinuma, Y., Yakoh, T., Aoyama, T., Anzai, H., Isobe, K., 2004. Development of gel-structured electro-rheological fluids and their application to mechanical damper elements. In: The 8th IEEE International Workshop on Advanced Motion Control. IEEE, pp. 541–545.

[23] Kamath, G. M., Wereley, N. M., 1997. A nonlinear viscoelastic-plastic model for electrorheological fluids. Smart Materials and Structures 6 (3), 351.

[24] Kamelreiter, M., Kemmetmüller, W., Kugi, A., 2012. Digitally controlled electrorheological valves and their application in vehicle dampers. Mechatronics 22 (5), 629–638.

[25] Kim, Y., Langari, R., Hurlebaus, S., 2009. Semiactive nonlinear control of a building with a magnetorheological damper system. Mechanical Systems and Signal Processing 23 (2), 300–315.

[26] Ljung, L., 1998. System identification. In: Signal analysis and prediction. Springer, pp. 163–173.

[27] Makris, N., Burton, S. A., Taylor, D. P., 1996. Electrorheological damper with annular ducts for seismic protection applications. Smart Materials and Structures 5 (5), 551.

[28] Marquardt, D. W., 1963. An algorithm for least-squares estimation of nonlinear parameters. Journal of the society for Industrial and Applied Mathematics 11 (2), 431–441.

[29] Martins, S. A. M., Aguirre, L. A., 2016. Sufficient conditions for rate-independent hysteresis in autoregressive identified models. Mechanical Systems and Signal Processing 75, 607–617.

[30] McClamroch, N. H., Gavin, H., 1995. Closed loop structural control using electrorheological dampers. In: American Control Conference, Proceedings of the 1995. Vol. 6. IEEE, pp. 4173–4177.

[31] Metered, H., Bonello, P., Oyadiji, S., 2010. The experimental identification of magnetorheological dampers and evaluation of their controllers. Mechanical systems and signal processing 24 (4), 976–994.

[32] Nakamura, T., Saga, N., Nakazawa, M., 2004. Variable viscous control of a homogeneous er fluid device considering its dynamic characteristics. Mechatronics 14 (1), 55–68.

[33] Nik Mohamed, N. A., Mohd Nor, M. J., Mukhlis, R. Z., 2016. Compromising vehicle handling and passenger ride comfort using er-damper. Mechanics 54 (4), 50–54.

[34] Papadopoulos, C. A., 1998. Brakes and clutches using ER fluids. Mechatronics 8 (7), 719–726.

[35] Peel, D., Bullough, W., 1994. Prediction of electro-rheological valve performance in steady flow. Proceedings of the Institution of Mechanical Engineers, Part C: Journal of Mechanical Engineering Science 208 (4), 253–266.

[36] Purdy, D., Bulman, D., 1997. An experimental and theoretical investigation into the design of an active suspension system for a racing car. Proceedings of the Institution of Mechanical Engineers, Part D: Journal of Automobile Engineering 211 (3), 161–173.

[37] Reineh, M. S., Pelosi, M., 2013. Physical modeling and simulation analysis of an advanced automotive racing shock absorber using the 1d simulation tool amesim. SAE International Journal of Passenger Cars-Mechanical Systems 6 (2013-01-0168), 7–17.

[38] Sammier, D., Sename, O., Dugard, L., 2003. Skyhook and h_∞ control of semi-active suspensions: some practical aspects. Vehicle System Dynamics 39 (4), 279–308.

[39] Savaresi, S. M., Poussot-Vassal, C., Spelta, C., Sename, O., Dugard, L., 2010. Semi-active suspension control design for vehicles. Elsevier.

[40] Spencer Jr, B., Dyke, S., Sain, M., Carlson, J., 1997. Phenomenological model for magnetorheological dampers. Journal of engineering mechanics 123 (3), 230–238.

[41] Stanway, R., Sproston, J., Stevens, N., 1985. Non-linear identification of an electrorheological vibration damper. In: IFAC Identification and System Parameter Estimation. Vol. 7. pp. 195–200.

[42] Stanway, R., Sproston, J., Stevens, N., 1987. Non-linear modelling of an electro-rheological vibration damper. Journal of Electrostatics 20 (2), 167–184.

[43] Sun, W., Li, J., Zhao, Y., Gao, H., 2011. Vibration control for active seat suspension systems via dynamic output feedback with limited frequency characteristic. Mechatronics 21 (1), 250–260.

[44] Vivas-Lopez, C., Alcántara, D. H., Nguyen, M. Q., Fergani, S., Buche, G., Sename, O., Dugard, L., Morales-Menéndez, R., 2010. INOVE: Integrated approach for observation and control of vehicle dynamics. `http://www.gipsa-lab.fr/projet/inove/index.html`, accessed: 13/10/2016.

[45] Vivas-Lopez, C., Alcántara, D. H., Nguyen, M. Q., Fergani, S., Buche, G., Sename, O., Dugard, L., Morales-Menéndez, R., 2014. INOVE: a testbench for the analysis and control of automotive vertical dynamics. In: 14th International Conference on Vehicle System Dynamics, Identification and Anomalies.

[46] Witters, M., Swevers, J., 2010. Black-box model identification for a continuously variable, electro-hydraulic semi-active damper. Mechanical Systems and Signal Processing 24 (1), 4–18.

[47] Yakoh, T., Aoyama, T., 2000. Application of electro-rheological fluids to flexible mount and damper devices. In: 26th Annual Confjerence of the IEEE Industrial Electronics Society. Vol. 3. IEEE, pp. 1815–1820.